

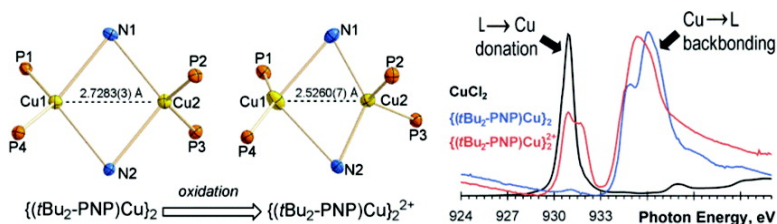
Article

**Probing the Electronic Structures of [Cu(□-XR)] Diamond Cores as a Function of the Bridging X Atom (X = N or P) and Charge ( $n = 0, 1, 2$ )**

Seth B. Harkins, Neal P. Mankad, Alexander J. M. Miller, Robert K. Szilagy, and Jonas C. Peters

*J. Am. Chem. Soc.*, **2008**, 130 (11), 3478-3485 • DOI: 10.1021/ja076537v

Downloaded from <http://pubs.acs.org> on February 8, 2009



**More About This Article**

Additional resources and features associated with this article are available within the HTML version:

- Supporting Information
- Links to the 2 articles that cite this article, as of the time of this article download
- Access to high resolution figures
- Links to articles and content related to this article
- Copyright permission to reproduce figures and/or text from this article

[View the Full Text HTML](#)

## Probing the Electronic Structures of $[\text{Cu}_2(\mu\text{-XR}_2)]^{n+}$ Diamond Cores as a Function of the Bridging X Atom (X = N or P) and Charge ( $n = 0, 1, 2$ )

Seth B. Harkins,<sup>†</sup> Neal P. Mankad,<sup>†,§</sup> Alexander J. M. Miller,<sup>†</sup>  
Robert K. Szilagyi,<sup>\*,‡</sup> and Jonas C. Peters<sup>\*,†,§</sup>

*Division of Chemistry and Chemical Engineering, Arnold and Mabel Beckman Laboratories of Chemical Synthesis, California Institute of Technology, Pasadena, California 91125, and Department of Chemistry and Biochemistry, Montana State University, Bozeman, Montana 59717*

Received September 1, 2007; E-mail: Szilagyi@Montana.edu; JPeters@MIT.edu

**Abstract:** A series of dicopper diamond core complexes that can be isolated in three different oxidation states ( $[\text{Cu}_2(\mu\text{-XR}_2)]^{n+}$ , where  $n = 0, 1, 2$  and X = N or P) is described. Of particular interest is the relative degree of oxidation of the respective copper centers and the bridging XR<sub>2</sub> units, upon successive oxidations. These dicopper complexes feature terminal phosphine and either bridging amido or phosphido donors, and as such their metal–ligand bonds are highly covalent. Cu K-edge, Cu L-edge, and P K-edge spectroscopies, in combination with solid-state X-ray structures and DFT calculations, provides a complementary electronic structure picture for the entire set of complexes that tracks the involvement of a majority of ligand-based redox chemistry. The electronic structure picture that emerges for these inorganic dicopper diamond cores shares similarities with the Cu<sub>2</sub>(μ-SR)<sub>2</sub> Cu<sub>A</sub> sites of cytochrome *c* oxidases and nitrous oxide reductases.

### Introduction

An emerging theme in transition-metal coordination chemistry is to consider the role of ligands in the stabilization of different oxidation states and to view such ligands as redox-active.<sup>1</sup> While this view is distinct from the traditional model where oxidation state changes are predominantly attributed to redox-active transition-metal centers, it is in accord with a covalent bonding description due to ligand-to-metal charge donation. Strong covalency is apparently exploited within the active sites of certain metalloenzymes.<sup>2</sup> Relevant to the present study, the bimetallic diamond core Cu<sub>A</sub> sites found in cytochrome *c* oxidases and nitrous oxide reductases serve as electron-transfer relays with highly covalent thiolate bridging units that are key to their function.<sup>3</sup> A relevant investigation of the Cu<sub>A</sub> center engineered into *Pseudomonas aeruginosa* azurin revealed the

presence of highly covalent bonding between the copper centers and the bridging thiolate (Cys) ligands.<sup>3c</sup> In the mixed-valence form of the Cu<sub>A</sub> site ( $[\text{Cu}_2(\mu\text{-SR})_2]$ ), spectroscopic and theoretical work have provided a picture of the electronic structure originating from four major contributions: total sulfur (46%) and β-methylene (3%) groups of the bridging cysteine ligands, total nitrogen (6%) of the terminal histidine ligands, and the two Cu centers (44%).

A biomimetic mixed-valence model complex that is structurally faithful by virtue of its thiolate bridges,  $[(\text{L}^{\text{iPrdaco}}\text{SCu})_2]^+$ ,<sup>4</sup> was suggested to have even more sulfur character: 54% μ-S and 38% Cu 3d contributions. This model system features copper centers at a distance (2.93 Å)<sup>4</sup> that is nonetheless substantially larger than that found in Cu<sub>A</sub> sites (~2.5 Å).<sup>5</sup> The numerical assignments for the relative degree of copper versus thiolate character within the redox-active molecular orbital/s (RAMOs) of Cu<sub>2</sub>(μ-SR)<sub>2</sub> mixed-valence systems suggest that strong covalency contributes to the unique electron transfer (ET) properties of Cu<sub>A</sub> sites. However, the  $[(\text{L}^{\text{iPrdaco}}\text{SCu})_2]^+$  model complex does not serve as a functional model of the Cu<sub>A</sub> site as it lacks the requisite, reversible one-electron redox couple between the Cu<sup>I</sup>Cu<sup>I</sup> and the Cu<sup>1.5</sup>Cu<sup>1.5</sup> states. To gain a better appreciation of how covalency gives rise to the desirable ET properties of Cu<sub>A</sub>

<sup>†</sup> California Institute of Technology.

<sup>‡</sup> Montana State University.

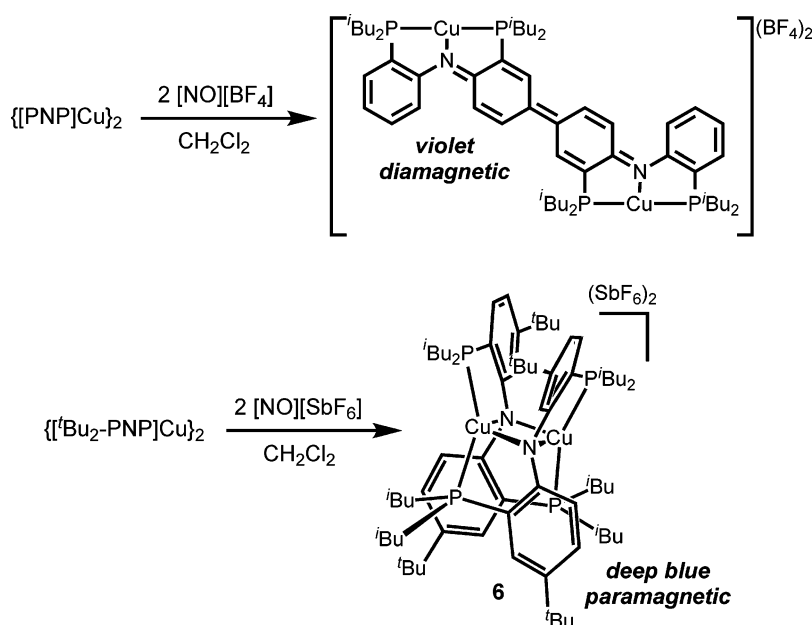
<sup>§</sup> Present address: Massachusetts Institute of Technology.

- (1) (a) Ray, K.; Bill, E.; Weyhermuller, T.; Wieghardt, K. *J. Am. Chem. Soc.* **2005**, *127*, 5641. (b) Bart, S. C.; Lobkovsky, E.; Bill, E.; Wieghardt, K.; Chirik, P. J. *Inorg. Chem.* **2007**, *46*, 7055. (c) Szilagyi, R. K.; Lim, B. S.; Glaser, T.; Holm, R. H.; Hedman, B.; Hodgson, K. O.; Solomon, E. I. *J. Am. Chem. Soc.* **2003**, *125*, 9158.
- (2) Holm, R. H.; Kennepohl, R.; Solomon, E. I. *Chem. Rev.* **1996**, *96*, 2239.
- (3) (a) Ferguson-Miller, S.; Babcock, G. T. *Chem. Rev.* **1996**, *96*, 2889. (b) Gamelin, D. R.; Randall, D. W.; Hay, M. T.; Houser, R. P.; Mulder, T. C.; Canters, G. W.; de Vries, S.; Tolman, W. B.; Lu, Y.; Solomon, E. I. *J. Am. Chem. Soc.* **1998**, *120*, 5246. (c) Ramirez, B. E.; Malmstrom, B. G.; Winkler, J. R.; Gray, H. B. *Proc. Natl. Acad. Sci. U.S.A.* **1995**, *92*, 11949. (d) Antholine, W. E.; Kastrau, D. H. W.; Steffens, G. C. M.; Buse, G.; Sumft, W. G.; Kroneck, P. M. H. *Eur. J. Biochem.* **1992**, *209*, 875. (e) DeBeer-George, S.; Metz, M.; Szilagyi, R. K.; Wang, J.; Cramer, S. P.; Lu, Y.; Tolman, W. B.; Hedman, B.; Hodgson, K. O.; Solomon, E. I. *J. Am. Chem. Soc.* **2001**, *123*, 5757.

(4) Houser, R. P.; Young, V. G., Jr.; Tolman, W. B. *J. Am. Chem. Soc.* **1996**, *118*, 2101.

(5) (a) Blackburn, N. J.; Barr, M. E.; Woodruff, W. H.; van der Oost, J.; de Vries, S. *Biochemistry* **1994**, *33*, 10401. (b) Williams, M.; Lapplalainen, P.; Kelly, M.; Sauer-Eriksson, E.; Saraste, M. *Proc. Natl. Acad. Sci. U.S.A.* **1995**, *92*, 11955.

Scheme 1



sites, it is of interest to probe in detail  $\text{Cu}_2(\mu\text{-X})_2$  sites that can be studied as a function of various formal oxidation states.

In this paper we describe two unique sets of dicopper complexes in which the  $\text{Cu}_2(\mu\text{-XR}_2)_2$  diamond core topologies are preserved across *three* formal oxidation states, providing a unique opportunity to explore factors affecting the properties of  $\text{Cu}_2(\mu\text{-XR}_2)_2$  systems. Synthetic, X-ray diffraction (XRD), and X-ray absorption spectroscopy (XAS) studies have been used to probe the relationship between the redox behavior, geometric structures, and electronic structures of these  $\text{Cu}_2(\mu\text{-XR}_2)_2$  cores on the bridging X unit ( $\text{X} = \text{N}$  vs  $\text{P}$ ) and the overall molecular charge ( $n = 0, 1, 2$ ). While the nature of the bridging ligands employed in this study is distinct from the thiolate units found in biological systems, striking electronic structural similarities are evident between the redox-active molecular orbitals of these inorganic model complexes and those that have been elucidated for the  $\text{Cu}_A$  site.

## Results and Discussion

For the purposes of this study, we required access to synthetically well-defined dicopper systems for which amido ( $\text{NR}_2^-$ )<sup>6,7</sup> or phosphido ( $\text{PR}_2^-$ )<sup>8</sup> units occupied the bridging positions and for which each series was stable across three oxidation states. The synthesis and X-ray crystal structures of the series of phosphide-bridged dicopper complexes  $\{(\text{PPP})\text{Cu}\}_2$  (**1**),  $\{(\text{PPP})\text{Cu}\}_2^+$  (**2**), and  $\{(\text{PPP})\text{Cu}\}_2^{2+}$  (**3**) ( $\text{PPP}^- = \text{bis}(2\text{-diisopropylphosphinophenyl})\text{phosphide}$ ) were communicated recently.<sup>8</sup> A structurally analogous, highly luminescent amido-bridged species  $\{(\text{PNP})\text{Cu}\}_2$  ( $\text{PNP} = \text{bis}(2\text{-diisobutylphosphinophenyl})\text{amide}$ ) has also been described.<sup>7</sup> Problematic for this latter system, however, is that only  $\{(\text{PNP})\text{Cu}\}_2$  and its monocation  $[\{(\text{PNP})\text{Cu}\}_2]^+$  can be isolated, despite the presence of two independent and reversible redox couples in the cyclic voltammetry data. Attempts to synthetically generate the dication,  $[\{(\text{PNP})\text{Cu}\}_2]^{2+}$ , by the addition of 2 equiv of an

oxidant such as  $[\text{NO}][\text{BF}_4]$  were not fruitful. Instead, an inky violet dicopper(I) degradation product, denoted herein as  $[\text{Cu}_2(\text{PNP-2H}_2)][\text{BF}_4]_2$ , was isolated in which C–C coupling of the  $[\text{PNP}]$  ligands had occurred at the aryl ring in a position para to the N atom (Scheme 1). The solid-state crystal structure of this degradation product, which features two isolated, three-coordinate copper(I) centers, is provided in the Supporting Information. Loss of  $\text{H}_2$  or some byproduct derived from formal loss of 2  $\text{H}\cdot$  can be inferred based upon the reaction product, though no attempt has yet been made to study this transformation more carefully.

For the purposes of this study, it was necessary to add stability to both the one- and two-electron oxidized species of the  $(\text{PNP})$  ligand system. To do this, a *tert*-butyl group para to the amido N atom has been incorporated into the  $(\text{PNP})$  ligand, and this latter derivative is abbreviated herein as  $(\text{tBu}_2\text{-PNP})$  (Figure 1).  $(\text{tBu}_2\text{-PNP})\text{H}$  can be prepared by literature methods,<sup>9</sup> and subsequent reaction with mesitylcopper affords yellow and highly emissive  $\{(\text{tBu}_2\text{-PNP})\text{Cu}\}_2$  (**4**) in good yield. The cyclic voltammogram of **4** exhibits two reversible redox processes at  $-0.49$  and  $+0.30$  V vs  $\text{Fc}^+/\text{Fc}$ . Both processes are anodically shifted relative to their corresponding couples in the  $\{(\text{PPP})\text{Cu}\}_2^{n+}$  system ( $-1.02$  and  $-0.42$  V).<sup>6</sup> The oxidation of **4** with 1 equiv of either  $[\text{FeCp}_2][\text{BAR}^{\text{F}}_4]$  ( $\text{Ar}^{\text{F}} = 3,5\text{-(CF}_3)_2\text{-C}_6\text{H}_3$ ) or  $\text{AgSbF}_6$  produces  $[\{(\text{tBu}_2\text{-PNP})\text{Cu}\}_2]^+$  (**5**) as red-brown crystals. The addition of 2 equiv of  $[\text{NO}][\text{SbF}_6]$  to **4** in  $\text{CH}_2\text{Cl}_2$  solution results in a deep blue color with an associated appearance of a sharp optical transition at  $16\,100\text{ cm}^{-1}$  ( $\epsilon = 10\,700\text{ M}^{-1}\text{ cm}^{-1}$ ). The dicationic product of this reaction,  $[\{(\text{tBu}_2\text{-PNP})\text{Cu}\}_2][\text{SbF}_6]_2$  (**6**), is sufficiently stable to be isolated in crystalline form. The X-band electron paramagnetic resonance (EPR) signal for monocation **5** features a very broad, featureless isotropic signal with  $g_x = 1.987$ ,  $g_y = 2.025$ , and  $g_z = 2.098$ . The absorption spectrum of **5** has a characteristic charge-transfer band at  $5330\text{ cm}^{-1}$  ( $\epsilon = 3200\text{ M}^{-1}\text{ cm}^{-1}$ ) that is believed to be predominantly ligand-to-ligand in character

(6) Harkins, S. B.; Peters, J. C. *J. Am. Chem. Soc.* **2004**, *126*, 2885.

(7) Harkins, S. B.; Peters, J. C. *J. Am. Chem. Soc.* **2005**, *127*, 2030.

(8) Mankad, N. P.; Rivard, E.; Harkins, S. B.; Peters, J. C. *J. Am. Chem. Soc.* **2005**, *127*, 16032.

(9) Ozerov, O. V.; Guo, C.; Papkov, V. A.; Foxman, B. M. *J. Am. Chem. Soc.* **2004**, *126*, 4792.

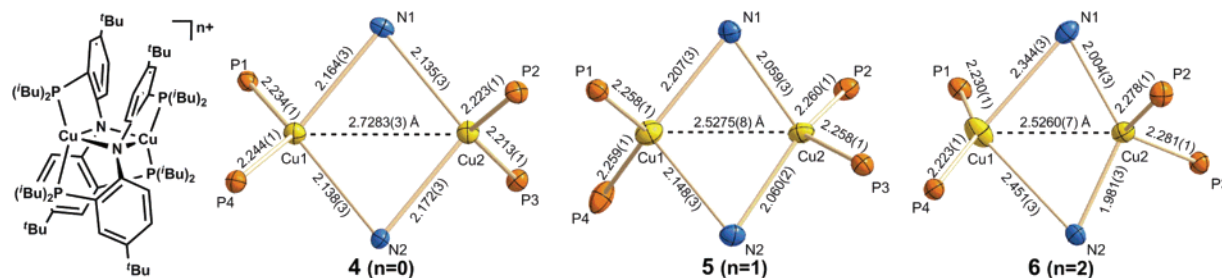


**Figure 1.** Thermal ellipsoid representations of the core atoms of neutral **4**, cation **5**, and dication **6**. See selected bond lengths (Å) above. Selected angles (deg) follow. For **4**: Cu1–N1–Cu2, 78.77(1); Cu1–N2–Cu2, 78.52(1); N1–Cu1–N2, 101.35(1); N1–Cu2–N2, 101.19(1). For **5**: Cu1–N1–Cu2, 73.75(8); Cu1–N2–Cu2, 72.56(8); N1–Cu1–N2, 102.03(1); N1–Cu2–N2, 110.5(1). For **6**: Cu1–N1–Cu2, 70.83(8); Cu1–N2–Cu2, 68.60(8); N1–Cu1–N2, 95.19(8); N1–Cu2–N2, 125.31(1).

(vide infra). Dication **6** is paramagnetic, contrasting its diamagnetic phosphide-bridged relative **3**.<sup>6</sup> X-band EPR data for **6** in a frozen dichloromethane/toluene (20:1) glass at 3.7 K show a broad signal at  $g = 1.998$  and a weak half-field signal at  $g = 4.02$ , consistent with an  $S = 1$  spin system. No hyperfine coupling information is resolvable over the temperature range of 3.7–154 K.

Figure 1 depicts the core ellipsoids obtained from high-quality X-ray crystal structures for **4**, cation **5** as its [BARF<sub>4</sub>] salt, and dication **6** as its [SbF<sub>6</sub>] salt. These three solid-state structures are to be compared with the previously reported set of crystal structures for the {(PPP)Cu}<sub>2</sub><sup>n+</sup> series **1–3**.<sup>6</sup> Immediately evident for **4–6** is a common topology that is also seen in **1–3**.<sup>6</sup> The Cu···Cu distance in **4** is 2.7283(3) Å, and it contracts by ca. 0.2 Å upon oxidation to **5**. While there is negligible change in the Cu···Cu distance between **5** and **6**, there is a dramatic asymmetric structural distortion of the Cu<sub>2</sub>(μ-NR<sub>2</sub>)<sub>2</sub> core resulting in two elongated Cu–N distances (2.34 and 2.45 Å) and two typical Cu–N distances (2.00 and 1.98 Å) for dicationic **6**.

The unexpected asymmetry in the structure of **6** brings up the possibility that the copper centers have different oxidation states. A simplistic analysis suggests a pseudo-two-coordinate Cu<sup>I</sup> center that is very weakly coordinated to the bridging amido units, and a four-coordinate Cu<sup>II</sup> or Cu<sup>III</sup> center much more tightly coordinated to the bridging amido units. The related, but diamagnetic phosphide-bridged dication, {(PPP)Cu}<sub>2</sub><sup>2+</sup> **3**,<sup>6</sup> has a symmetric Cu<sub>2</sub>(μ-PR<sub>2</sub>)<sub>2</sub> core structure that can mostly simply be described by two antiferromagnetically coupled Cu<sup>II</sup> centers. Hence, the relative oxidation states between the monocations **2** and **5** and the dications **4** and **6** appear to depend on the chemical nature of the bridging XR<sub>2</sub> unit. But due to the expected highly covalent bonding, redox chemistry likely affects redox active molecular orbitals (RAMOs) with significant Cu and bridging XR<sub>2</sub> unit contributions. Such an orbital was initially identified by a DFT study of {(SNS)Cu}<sub>2</sub><sup>+</sup> ((SNS) = bis(2-*tert*-butylsulfanylphenyl)amido).<sup>6</sup> Hence, a more careful analysis is needed to establish the relative degree of oxidation of the copper centers and the bridging ligands as electrons are removed from these Cu<sub>2</sub>(μ-XR<sub>2</sub>)<sub>2</sub> systems.

To experimentally investigate the RAMOs of **1–6**, we undertook a multi-edge X-ray absorption spectroscopic study at the Cu K-, Cu L-, and P K-edges. These edges directly probe the orbital composition (metal and ligand covalency) of the frontier unoccupied orbitals and the effective oxidation states of the Cu and P atoms.<sup>10</sup> Effective oxidation states that are

experimentally determined by a change in the effective nuclear charges of a system can differ substantially from formal oxidation state assignments due to considerable donation/removal of electron density by the metal's donor ligands. The effective nuclear charges and relative differences in effective oxidation states can be generally obtained by examining the rising K-edge inflection points of the metal center in question and the K-edges of the donor atoms coordinated to the metal. As shown in Figures 2A and 3A, the rising-edge inflection points of the Cu K-edge spectra of **1** and **4** are between the reference spectra for Cu<sup>I</sup>(pyridine)<sub>4</sub><sup>+</sup> (8986.1 eV) and Cu<sup>II</sup>Cl<sub>2</sub> (8991.6 eV).<sup>11</sup> Upon oxidation, the inflection points shift to higher energy by less than 0.5 eV for **1–5**. The small variation in the energy of the inflection points lies approximately within the resolution of the XAS technique at ~9000 eV. Therefore, by this measure the Cu centers in complexes **1–5** appear to have similar effective oxidation states. The Cu K-edge spectrum of the dication **6** (red trace) shows a 1.7 eV shift relative to neutral **4** (blue trace), which could be a result of substantial differences in their effective oxidation states. To evaluate this possibility, we estimated the Cu K-edge spectra of complexes with formally four- and two-coordinate Cu<sup>I</sup> centers (Figure 4A) and also a complex with four-coordinate Cu<sup>I</sup> and Cu<sup>III</sup> centers (Figure 4B). Comparison of the measured spectrum of **6** with these estimated spectra shows a close similarity between that for **6** and the four- and two-coordinate copper centers. We therefore conclude that the 1.7 eV shift that is observed in the Cu K-edge of **6** results from the superposition of the K-edges of pseudo four- and two-coordinate copper(I) centers, rather than from substantial oxidation of the copper centers.

Figures 2B and 3B show two groups of spectral features at the Cu L<sub>3</sub>-edge. The pre-edge features at around 932 eV arise due to unoccupied Cu 3d orbital character. For the (PPP) series, the neutral complex **1** shows no preedge at 931 eV (purple trace) due to its filled 3d-shell. Pre-edge transitions arise at 933.3 eV upon single and double oxidation steps to **2** (olive) and **3** (orange). For the (tBu<sub>2</sub>-PNP) series, the neutral complex **4** shows essentially no preedge feature (blue) due to the 3d<sup>10</sup> configuration. As this complex is oxidized (green), a small pre-edge feature emerges at 931.7 eV indicating limited metal character in the RAMO. For the reference Cu<sup>II</sup>Cl<sub>2</sub> spectrum the pre-edge feature corresponds to 71% Cu 3d character.<sup>12</sup> By comparing the area of the pre-edge feature of **5** with that for

(11) Kau, L. S.; Spira-Solomon, D. J.; Pennerhahn, J. E.; Hodgson, K. O.; Solomon, E. I. *J. Am. Chem. Soc.* **1987**, *109*, 6433.

(12) (a) Gewirth, A. A.; Cohen, S. L.; Schugar, H. J.; Solomon, E. I. *Inorg. Chem.* **1987**, *26*, 1133. (b) Didziulis, S. V.; Cohen, S. L.; Gewirth, A. A.; Solomon, E. I. *J. Am. Chem. Soc.* **1988**, *110*, 250.

(10) Solomon, E. I.; Hedman, B.; Hodgson, K. O.; Dey, A.; Szilagy, R. K. *Coord. Chem. Rev.* **2005**, *249*, 97.

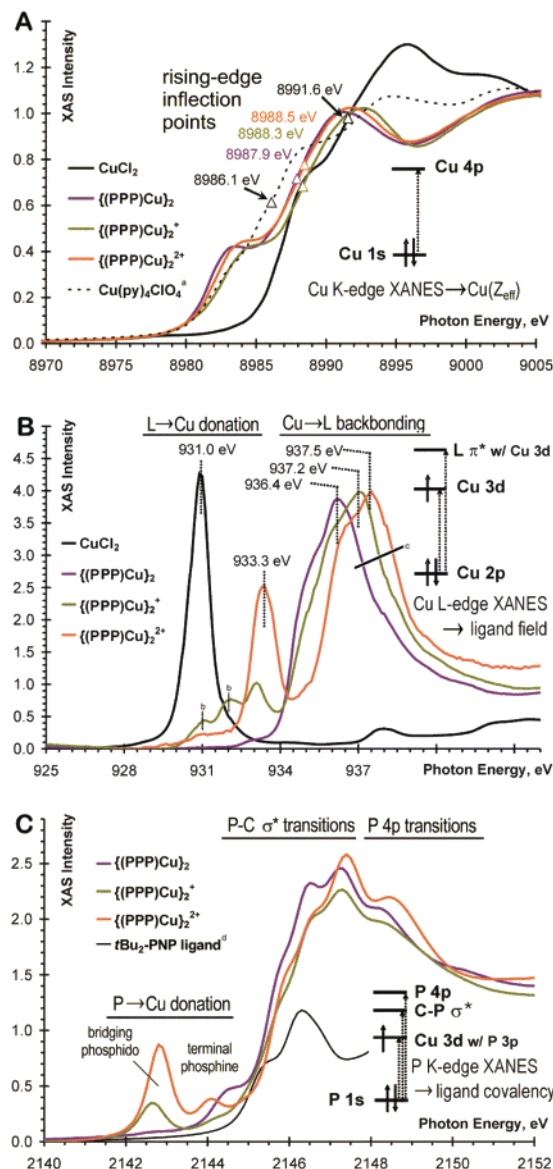


**Figure 2.** Multi-edge (Cu K-edge, A; Cu L-edges, B; P K-edge, C) X-ray absorption spectra for  $\{(\text{PPP})\text{Cu}_2\}^{n+}$ ,  $n = 0$  (1), 1 (2), 2 (3). Key to notes: (a) Taken from ref 11. (b) The pre-edge features of  $\{(\text{PPP})\text{Cu}_2\}^{2+}$  at  $\sim 931$  and  $\sim 932$  eV are due to the presence of endogenous  $\text{Cu}^{\text{II}}$  species and partially oxidized mesitylcopper(I) impurity. (c) A similar group of features are also present at the  $\text{Cu}$   $L_2$ -edge, which indicates that they originate from Cu-based transitions. (d) The  $(\text{tBu}_2\text{-PNP})$  ligand spectrum is renormalized by 0.5 relative to the spectra of the other complexes shown, as it contains only half as many phosphorus absorbers.

$\text{CuCl}_2$ , approximately 24% Cu 3d character can be assigned to the RAMO of **5**. For comparison, the Cu 3d character in the thiolate-bridged, mixed-valence model complex  $[(\text{L}^{\text{iPr}}\text{Pr}^{\text{daco}}\text{S})\text{Cu}_2]^+$  was estimated at 38%.<sup>3e</sup> Upon further oxidation of **5**, another electron hole is opened in the RAMO-1 orbital (red, 931 eV). The comparatively small amount of Cu orbital character indicated by these Cu  $L_3$ -edge features supports the assignment of a substantial degree of ligand-based redox chemistry upon one- and two-electron oxidation steps in both the (PPP) and  $(\text{tBu}_2\text{-PNP})$  series.

Transitions at 934–937 eV suggest a considerable amount of  $\text{Cu} \rightarrow \text{L}$  backdonation, presumably into the  $\pi^*$  manifold of the aryl rings. Solomon et al. have recently observed related spectral features that result from backbonding contributions by

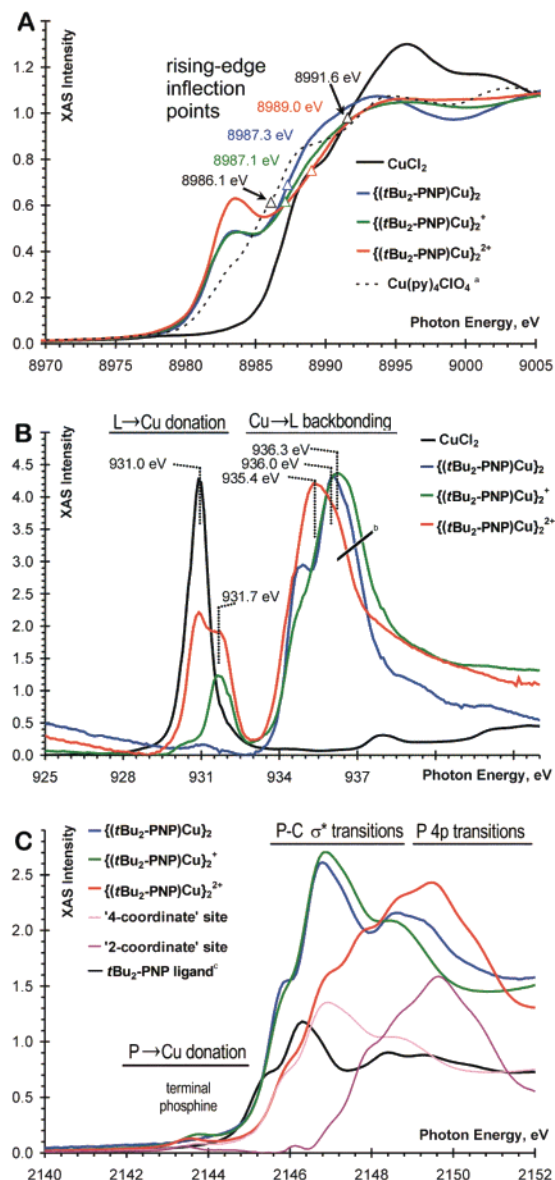


**Figure 3.** Multi-edge (Cu K-edge, A; Cu L-edges, B; P K-edge, C) X-ray absorption spectra for  $\{(\text{tBu}_2\text{-PNP})\text{Cu}_2\}^{n+}$ ,  $n = 0$  (4), 1 (5), 2 (6). Key to notes: (a) Taken from ref 11. (b) A similar group of features is also present at the  $\text{Cu}$   $L_2$ -edge, which indicates that they originate from Cu-based transitions. (c) The  $(\text{tBu}_2\text{-PNP})$  ligand spectrum is renormalized by 0.5 relative to the spectra of the other complexes shown, as it contains only half as many phosphorus absorbers.

Fe L-edge XAS for  $[\text{Fe}(\text{CN})_6]^{3/4-}$ .<sup>13</sup> In addition, we have recently suggested that donation from an amido lone pair, admixed with Cu 3d-character, into an orbital of aryl  $\pi^*$  character is likely to be one key element that gives rise to the unusual emission characteristics of copper(I) arylamidophosphine complexes.<sup>14</sup> The observation of strong backbonding contributions in these Cu  $L_3$ -edge spectra is consistent with such a suggestion. Moreover, the presence of these features at similar energies and intensities in *all* of the spectra suggests that the copper centers maintain considerable  $\text{Cu}^{\text{I}}$  character as electrons are removed from the dinuclear systems. Note also that the single and double pre-edge features at 933.3 and 931–931.7

(13) Hocking, R. K.; Wasinger, E. C.; de Groot, F. M. F.; Hodgson, K. O.; Hedman, B.; Solomon, E. I. *J. Am. Chem. Soc.* **2006**, *128*, 10442.

(14) Miller, A. J.; Dempsey, J. L.; Peters, J. C. *Inorg. Chem.* **2007**, *46*, 7244.

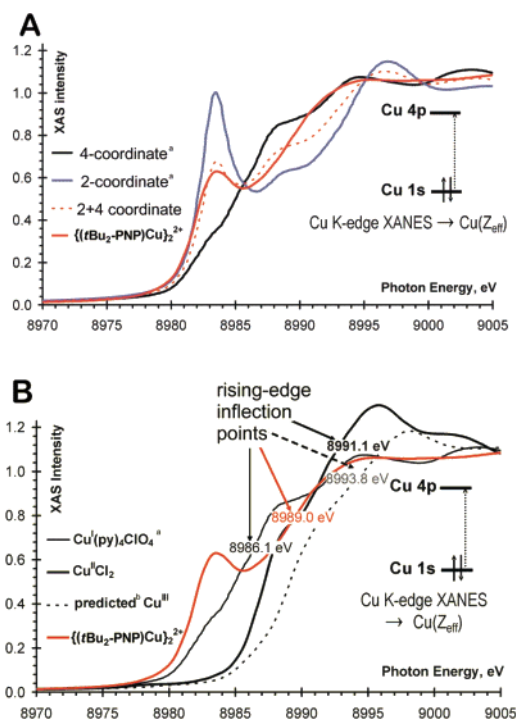


**Figure 4.** Predicted Cu K-edge spectra of a  $\text{Cu}_2\text{L}_2$  complex from (A) two-coordinate and four-coordinate  $\text{Cu}^{\text{I}}$  complexes and (B) from four-coordinate  $\text{Cu}^{\text{I}}$  and  $\text{Cu}^{\text{III}}$  complexes. Key to notes: (a) Data for B were taken from ref 11. (b) The four-coordinate  $\text{Cu}^{\text{III}}$  spectrum was predicted from an averaged +2 eV shifted  $\text{CuCl}_2$  and a +4 eV shifted  $\{\text{Cu}(\text{pyridine})_4\}\{\text{ClO}_4\}$ . These relative energy changes were estimated from edge shift positions given in ref 26. The approximately 2 eV blue shift corresponds to the effective nuclear charge increase upon one electron oxidation.

eV for **3** (orange trace) and **6** (red trace) reflect their singlet vs triplet ground states, respectively. The inflection points for the  $(\text{tBu}_2\text{-PNP})$  series are ca. 1 eV lower in energy than for the (PPP) series, indicative of more cuprous character in the amido-bridged set.

The P K-edge spectra of **1–3** and **4–6** in Figures 2C and 3C, respectively, reflect the orbital contributions from phosphorus ligands. The weak pre-edge features at 2143.5 eV in Figure 3C are indicative of modest terminal  $\text{P}(3\text{p})\text{-Cu}(3\text{d})$  covalent interactions. These pre-edge features appear to be slightly weaker in complexes **4–6**; however, this is due to their larger separation at 2144 eV (Figure 2C) from the rising-edge compared to **1–3**. The smaller  $\text{P}\rightarrow\text{Cu}$  donation is likely compensated by an increased bridging amido  $\text{N}\rightarrow\text{Cu}$  donation in **4–6** relative to bridging phosphido  $\text{P}\rightarrow\text{Cu}$  donation in **1–3**. The increased donation is already reflected by the ca. 0.2 Å shorter  $\text{Cu-N}$  bonds, relative to the  $\text{Cu-P}$  bonds, even considering the greater delocalization of the  $\mu\text{-N}$  (Figure 5B,C) than the  $\mu\text{-P}$  (Figure 5A) into the aromatic carbon rings. The rising edge shifts between the free  $(\text{tBu}_2\text{-PNP})\text{H}$  ligand and complexes **4–6** are due to the terminal  $\text{P}\rightarrow\text{Cu}$  4s/4p interactions. The larger shift and different rising-edge structure for the most oxidized complex **6** is due to the presence of two distinct coordination sites. The four-coordinate site has smaller P covalency relative to the pseudo-two-coordinate site due to stronger interaction with the  $\mu\text{-amido}$  group. The pseudo-two-coordinate Cu site receives electron density dominantly from the terminal phosphines, which increases the effective nuclear charge of these P atoms and shifts their spectral features to higher energy, by about 3 eV. In Figure 3C, the pink spectrum

is the 50% scaled spectrum of the  $\{(\text{tBu}_2\text{-PNP})\text{Cu}\}_2^+$  (green spectrum). It matches quite well with the rising edge features of **6** up to 2147 eV. This suggests that the  $\text{Cu-P}$  interactions of the four-coordinate site in **6** are similar to those in the one-electron more reduced complex **5**. The violet spectrum in Figure 3C is the difference spectrum between the red and pink spectra and thus corresponds to the pseudo-two-coordinate Cu site. The three shoulders at 2148.0, 2148.8, and 2149.6 eV can be correlated with the  $\text{Cu-P}$  bonding interaction and the  $\text{C-P}$   $\sigma^*$  interactions. The shortening of the  $\text{Cu-P}$  distances in the pseudo-two-coordinate site relative to the pseudo-four-coordinate site, as observed in their respective X-ray crystal structures, are in accord with these spectral observations.

The  $\text{Cu-P}$  bond distances are symmetric in the (PPP) series **1–3**, and the rising edges in Figure 2C are rather featureless. The small pre-edge features closer to the rising edge at 2144 eV reflect a weak terminal  $\text{P}(3\text{p})\text{-Cu}(3\text{d})$  covalent interaction. However, the P K-edge spectra of the (PPP) series show a second, more intense pre-edge feature at 2142.5 eV that corresponds to the  $\mu\text{-PR}_2\rightarrow\text{Cu}$  3d bonding interaction. As the (PPP) complexes are oxidized, this pre-edge feature gradually increases, confirming considerable  $\mu\text{-PR}_2$  character in the RAMO. An independent theoretical study of **1–3** by Head-Gordon and co-workers provides further support for the non-innocent nature of the (PPP) ligand system and strongly suggests that oxidation at the covalent bridging  $\mu\text{-PR}_2$  unit dominates, rather than oxidation of the aryl rings.<sup>15</sup> As they point out, our observation<sup>6</sup> of a strongly downfield-shifted  $^{31}\text{P}$  NMR  $\mu\text{-P}$  signal (266.1 ppm) for dication **3**, compared to that for neutral **1** (–21.0 ppm), provides independent experimental evidence that the phosphide units are being oxidized upon electron removal.

The experimentally probed RAMOs for **1–6** were also examined by electronic structure calculations. Orbital plots clearly show large bridging atom contributions. For example, for complexes **1** and **4** the bridging atom contributions are ~44% and ~35%, respectively, contrasting the modest terminal phosphorus contributions of 14% and 11% (Figure 5). Furthermore, for **1** and **4** about 22% and 38% C and H characters are delocalized into the aromatic  $\pi$  systems of the (PPP) and (PNP) ligands, respectively. This leaves approximately 18% and 16% Cu 3d character equally shared between the two metal sites, to be compared with the experimental estimate of Cu 3d character of approximately 24% per orbital from the Cu L-edge data (Figures 2B and 3B; see also discussion above). It is important to emphasize that the direct correlation between the experimental metal–ligand covalencies and calculated molecular orbital coefficients is limited by the lack of a transition dipole integral for the P 1s  $\rightarrow$  3p transition. Nonetheless, the orbital compositions of the  $\text{Cu}_2(\mu\text{-XR}_2)_2$  cores presented herein are qualitatively similar to those described for the  $\text{Cu}_A$  site.<sup>3e</sup>

The spin density plot for triplet **6** is shown in Figure 5D also indicates that the electron density corresponding to the two unpaired electrons is predominantly located (1.65 electrons) on the ligands. Furthermore, the spin density contour plot clearly shows the large difference between the two Cu coordination environments, a difference that is also reflected by the drastic changes in the Cu K- and P K-edge spectra (parts A and B of Figure 3, respectively) relative to **4** and **5**.

(15) Rhee, Y. M.; Head-Gordon, M., submitted for publication.

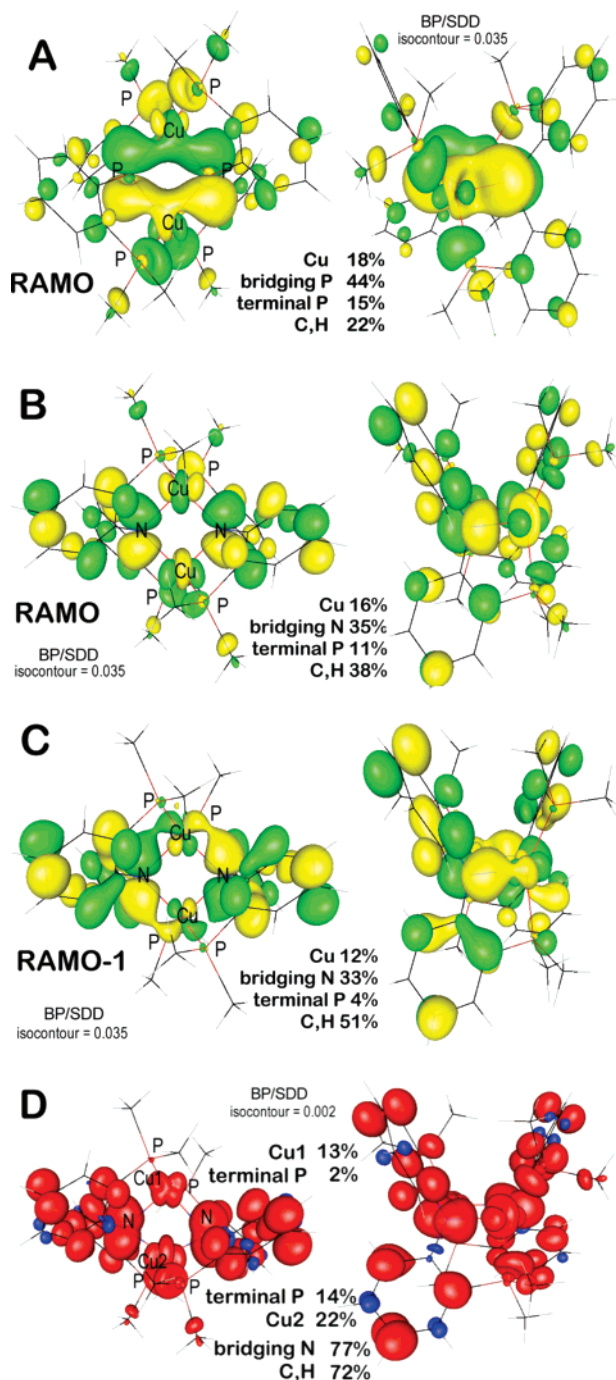


**Figure 5.** Molecular orbital plots of the redox-active orbitals (green and yellow) of **1** (A, HOMO) and **4** (B, HOMO; C, HOMO - 1); spin density plot (red and blue) for the triplet  $\{(\text{Bu}_2\text{-PNP})\text{Cu}\}_2^{2+}$  complex (D).

## Conclusions

The combined XAS and DFT data appear to rule out the possibility of **6** being a valence-trapped complex with  $\text{Cu}^{\text{III}}$  and  $\text{Cu}^{\text{I}}$  sites. The small shift of the rising-edge positions at the Cu K-edge, the lack of intense pre-edge features at the Cu L-edge, and the increasing pre-edge intensities at the P K-edge indicate in sum similar  $\text{Cu}^{\text{I}}$  character in each  $\text{Cu}_2(\mu\text{-XR}_2)_2$  core independent of the overall charge and the bridging group.

The dramatic contraction of the  $\text{Cu}\cdots\text{Cu}$  distances (0.2–0.5 Å) upon oxidation is one fascinating structural feature of these dicopper systems. A contributing electronic factor for the (PPP) series, where the contraction is most dramatic, is likely to be

the loss of  $\pi$ -bonding interactions between the  $\mu\text{-P}$  3p orbitals, mediated by overlap with Cu 3d orbitals (see Figure 5A).

In summation, the redox chemistry in these (PPP) and ( $\text{Bu}_2\text{-PNP}$ ) dicopper complexes features a strong ligand contribution, with a majority of the redox chemistry occurring at the bridging N or P atoms. The effective oxidation states of the Cu centers remain relatively constant throughout the two-electron-transfer series, lying closest to the cuprous state. The more reduced effective Cu oxidation states relative to the formal oxidation states originate from the combined effect of metal-to-ligand backdonation and substantial ligand-based redox due to the highly covalent nature of the  $\text{Cu}_2(\mu\text{-NR}_2)_2$  and  $\text{Cu}_2(\mu\text{-PR}_2)_2$  core units. These inorganic model diamond cores thus represent close analogues of the  $\text{Cu}_2(\mu\text{-SR})_2$  diamond core unit of the  $\text{Cu}_A$  site.

## Experimental Section

**General.** All manipulations were carried out using standard Schlenk or glovebox techniques under a dinitrogen atmosphere. Unless otherwise noted, solvents were deoxygenated and dried by thorough sparging with  $\text{N}_2$  gas followed by passage through an activated alumina column. Nonhalogenated solvents were tested with a standard purple solution of sodium benzophenone ketyl in tetrahydrofuran to confirm effective oxygen and moisture removal. All reagents were purchased from commercial vendors and used without further purification unless otherwise stated. Mesitylcopper(I),<sup>16</sup> diethylphosphoramidous dichloride,<sup>17</sup> 4,4'-di-*tert*-butyldiphenylamine,<sup>18</sup> and  $[\text{Cp}_2\text{Fe}][\text{B}(\text{C}_6\text{H}_3(\text{CF}_3)_2)_4]$ <sup>19</sup> were prepared according to literature procedures. Elemental analyses were performed by Desert Analytics, Tucson, AZ. Deuterated solvents were purchased from Cambridge Isotope Laboratories, Inc., and degassed and dried over activated 3 Å molecular sieves prior to use. A Varian Mercury-300 or INOVA-500 NMR spectrometer was used to record  $^1\text{H}$ ,  $^{13}\text{C}$ ,  $^{19}\text{F}$ , and  $^{31}\text{P}$  NMR spectra at ambient temperature.  $^1\text{H}$  chemical shifts were referenced to residual solvent.  $^{19}\text{F}$  chemical shifts were referenced to external  $\text{C}_6\text{F}_6$  ( $\delta = -165$  ppm), and  $^{31}\text{P}$  chemical shifts were referenced to external phosphoric acid ( $\delta = 0$  ppm). GC-MS data was obtained by injecting a dichloromethane solution into an Agilent 6890 GC equipped with an Agilent 5973 mass selective detector (EI). High-resolution EI mass spectroscopy was carried out by the Caltech Chemistry Mass Spectral Facility using a JEOL JMS600 instrument. UV-vis measurements were taken on Cary 500 UV-vis-NIR or Cary 50 UV-vis spectrophotometers using 1.0 or 0.1 cm quartz cells with a Teflon stopper. XRD studies were carried out in the Beckman Institute Crystallographic Facility on a Bruker Smart 1000 CCD diffractometer, and special refinement details are listed in the comments sections of the CIF files (Supporting Information). Magnetic measurements were undertaken at the Molecular Materials Research Center at the California Institute of Technology. Photophysical data were gathered at the Beckman Institute Laser Resource Center.

**EPR Measurements.** X-band EPR spectra were obtained on a Bruker EMX spectrometer (controlled by Bruker *Win EPR* software, version 3.0) equipped with a rectangular cavity working in the TE102 mode. Variable-temperature measurements were conducted with an Oxford continuous-flow helium cryostat (temperature range 3.6–300 K). Accurate frequency values were provided by a frequency counter built into the microwave bridge. Solution spectra were acquired in 2-methyltetrahydrofuran or 20:1 dichloromethane/toluene solution. Sample preparation was performed under a dinitrogen atmosphere in an EPR tube equipped with a ground glass joint.

**Electrochemistry.** Electrochemical measurements were carried out in a glovebox under a dinitrogen atmosphere in a one-compartment

(16) Eriksson, H.; Håkansson, M. *Organometallics* **1997**, *16*, 4243.

(17) Perich, J. W.; Johns, R. B. *Synthesis* **1998**, *2*, 142.

(18) Zhao, H.; Tanjutco, C.; Thayumanavan, S. *Tetrahedron Lett.* **2001**, *42*, 4421.

(19) Chavez, I. J. *Organomet. Chem.* **2000**, *601*, 126.

cell using a CH Instruments 600B electrochemical analyzer. Platinum wire was used as both the working and auxiliary electrodes. The reference electrode was Ag/AgNO<sub>3</sub> in THF. The ferrocene couple Fc<sup>+/0</sup> was used as an external reference. THF solutions of electrolyte (0.35 M tetra-*n*-butylammonium hexafluorophosphate) and analyte were also prepared under an inert atmosphere.

**Details of XAS Data Collection.** The copper K-, phosphorus K-, and copper L-edge XAS measurements were carried out at BL2-3, BL6-2, and BL10-1, respectively, of Stanford Synchrotron Radiation Laboratory under storage ring (SPEAR 3) conditions of 3 GeV energy and 100–80 mA current. BL2-3 is a 1.3 T bend magnet beam line and equipped with a Si(220) downward reflecting, double-crystal monochromator. Data was collected in the energy range of 8660–9690 eV using an unfocused beam and a 13-element Ge fluorescence detector array for samples placed in a liquid He cryostat. The beam intensity was maximized at 9685 eV. BL6-2 is a 56-pole, 0.9 T Wiggler beam line with a liquid-nitrogen-cooled, Si(111) double-crystal monochromator. P K-edge spectra were collected in the energy range of 2120–2250 eV using an unfocused beam in a He-purged fly path at room temperature and a Lytle fluorescence detector. The beam line was optimized at 2320 eV. BL10-1 has a 30-pole 1.45 T Wiggler insertion device with 6 m spherical grating monochromator. The samples were placed in a vacuum chamber with typical pressures of 10<sup>-6</sup> to 10<sup>-8</sup> torr, and the energy was scanned between 925 and 955 eV. The incident beam intensity and beam line optics were optimized at 920 eV. Data collection was carried out in electron yield mode by a Channeltron detector with 1.5 kV accelerating potential.

The solid samples were ground and pasted onto a contaminant-free Kapton tape from Shercon or carbon tape from Specs CertiPrep in a glovebox with sub parts per million oxygen and moisture levels. Samples for hard X-ray transmission measurements were diluted in and ground together with boronitride to minimize incident beam absorption. Samples were protected by a thin polypropylene window (Specs CertiPrep) from exposure to air during sample mounting and change. Sample holders for Cu L-edge measurements were mounted in a He-purged glovebag tightly wrapped around the vacuum chamber. The incident photon energy was scanned in 0.5 eV steps outside the rising edge region where the step-size was 0.1 eV. At least five scans were averaged to obtain a good signal-to-noise ratio. The incident photon energy was calibrated to the spectra of copper foil at the Cu K-edge (first inflection point at 8979 eV), difluorocopper(II) at the Cu L<sub>3</sub>- and L<sub>2</sub>-edges (white line positions at 930.5 and 950.5 eV, respectively), and triphenylphosphineoxide at the P K-edge (maximum of pre-edge feature at 2147.5 eV).

**Electronic Structure Calculations.** Density functional calculations were carried out using the *Gaussian03* suite.<sup>20</sup> The electronic structures of the computational models [(PXP)Cu]<sub>2</sub><sup>n+</sup>, where *n* = 0, 1, 2 and X = N or P in the bis(2-dimethylphosphinophenyl)amide or phosphide, respectively, which is a slightly truncated version of the (Bu<sub>2</sub>-PXP) ligand described in the manuscript; their ionic fragments were calculated by employing a gradient-corrected density functional composed of Becke nonlocal and Slater local density functional exchange<sup>21</sup> and Perdew nonlocal and Vosko-Wilk-Nussair local density functional correlation<sup>22</sup> functions (BP or BP86). Calculations were carried out using Stuttgart–Dresden effective core potential and corresponding valence triple- $\zeta$  basis set (ECP2).<sup>23</sup> We have utilized an ionic-fragment-based approach<sup>24</sup> to achieve rapid wave function convergence and to compare and contrast the possibility of various formal oxidation states.

The molecular orbital diagrams were generated using the Cube utility in *Gaussian* and the *GOpenMol*<sup>25</sup> visualizer program.

**Synthesis of [Cu<sub>2</sub>(PNP-2H)<sub>2</sub>][BF<sub>4</sub>]<sub>2</sub>.** NOBF<sub>4</sub> (22.5 g, 0.192 mmol) and {(PNP)Cu}<sub>2</sub> (100 mg, 0.096 mmol) were combined in chlorobenzene and stirred for 18 h, after which the solution had become inky purple in color. The solution was filtered through a glass microfilter and layered with petroleum ether. Upon standing for 4 days, analytically pure, X-ray-quality crystals were obtained (86 mg, 74%). The room-temperature NMR of the crystalline material is poorly resolved, likely due to a fluxional interaction of the BF<sub>4</sub> counterion and the Cu centers. This is evident from very broad <sup>19</sup>F NMR resonances rather than the sharp signal that is expected for an uncoordinated anion. <sup>1</sup>H NMR (300 MHz, CD<sub>2</sub>Cl<sub>2</sub>):  $\delta$  8.7 (br d), 8.51 (br d), 8.2 (br d), 7.8–7.3 (m), 6.93 (s), 2.45–1.55 (m), 1.11 (d), 1.03 (d), 0.98–0.92 (m). <sup>19</sup>F NMR (282 MHz, CD<sub>2</sub>Cl<sub>2</sub>):  $\delta$  -108.0 (br s), -125.5 (br s). <sup>31</sup>P{<sup>1</sup>H} NMR (121 MHz, CD<sub>2</sub>Cl<sub>2</sub>):  $\delta$  -27–-31 (m), -32.8 (s). Anal. Calcd for C<sub>56</sub>H<sub>86</sub>B<sub>2</sub>-Cu<sub>2</sub>F<sub>8</sub>N<sub>2</sub>P<sub>4</sub>: C, 55.41; H, 7.31; N, 2.31. Found: C, 55.01; H, 7.38; N, 2.26. UV-vis (CD<sub>2</sub>Cl<sub>2</sub>, nm(M<sup>-1</sup> cm<sup>-1</sup>)): 293 (7370), 327 (sh), 570 (sh), 613 (16250).

**Synthesis of Diisobutylchlorophosphine.** Neat diethylphosphorimidous dichloride (58.0 g, 0.333 mol) was added to a 2.0 M solution of isobutyl magnesium chloride in diethyl ether (350 mL) at 0 °C over a period of 30 min. Following addition, the solution was stirred at ambient temperature for 1 h and the crude <sup>31</sup>P NMR results indicated that the starting material had been consumed (<sup>31</sup>P NMR: 47.9 ppm, (Et)<sub>2</sub>NP(*i*Bu)<sub>2</sub>) and diisobutylchlorophosphine was the only phosphorus-containing product. The solution was again cooled to 0 °C, and a 2.0 M solution of anhydrous HCl in ether (350 mL) was added via cannula while stirring vigorously. A considerable amount of solid precipitated over a 2 h period, and the supernatant was isolated by cannula filtration. The solids were extracted with 200 mL of diethyl ether, and the solvent was removed by fractional distillation. The crude viscous oil was purified by fractional vacuum distillation (26–29 °C at 0.005 Torr) followed by removal of the residual diethyl ether by prolonged exposure to vacuum at -10 °C with stirring. The product was isolated as a spectroscopically pure, colorless oil (38.6 g, 65%) which exhibited a single resonance by <sup>31</sup>P NMR spectroscopy consistent with previously published results.<sup>18</sup> <sup>1</sup>H NMR (300 MHz, C<sub>6</sub>D<sub>6</sub>):  $\delta$  1.87 (m, 2H), 1.78 (br m, 2H), 1.24 (br m, 2H), 0.90 (br s, 12H). <sup>31</sup>P{<sup>1</sup>H} NMR (121 MHz, C<sub>6</sub>D<sub>6</sub>):  $\delta$  109.9.

**Synthesis of Di(2-bromo-4-*tert*-butylphenyl)amine.** In air, neat Br<sub>2</sub> (3.6 mL, 0.071 mol) at ~5 °C was added dropwise to a slurry of 4,4'-di-*tert*-butylphenylamine (10.0 g, 0.0356 mol) in acetic acid at ~16 °C. Following addition, the solution was stirred at ambient temperature for 2 h, a dilute solution of Na<sub>2</sub>S<sub>2</sub>O<sub>4</sub> (500 mL) was added, and the resulting solution was stirred for 15 min. The solids were collected on a frit and washed with H<sub>2</sub>O (3 × 200 mL). The crude product was purified by crystallization at -20 °C from methanol/chloroform as a white solid (12.35 g, 80%). <sup>1</sup>H NMR (300 MHz, CDCl<sub>3</sub>):  $\delta$  7.59 (m, 2H), 7.23 (m, 4H), 6.30 (br s, 1H) 1.32 (s, 18H). <sup>13</sup>C{<sup>1</sup>H} NMR (75.5 MHz, CDCl<sub>3</sub>): 145.9, 137.9, 130.2, 125.3, 117.8, 114.1, 34.5, 31.5. GC-MS(ES): 439 (M), 424 (M - CH<sub>3</sub>).

**Synthesis of Bis(2-diisobutylphosphino-4-*tert*-butylphenyl)amine, (Bu<sub>2</sub>-PNP)H.** A 1.6 M solution of *n*-butyl lithium in hexane (26 mL) was added dropwise to a solution of di(2-bromo-4-*tert*-butylphenyl)amine (6.0 g, 13.7 mmol) in diethyl ether (100 mL) at -70 °C with stirring. The solution immediately became yellow in color and was stirred at ambient temperature for 4 h at which time a precipitate formed. The reaction mixture was again cooled to -70 °C, at which time diisobutylchlorophosphine (7.67 g, 41.7 mmol) was added as a 1:1 solution with diethyl ether and the reaction was allowed to warm to room temperature. After 36 h at ambient temperature, a large amount

(20) Frisch, M. J. et al. *Gaussian03*, Gaussian, Inc.: Pittsburgh PA, 2004.

(21) Becke, A. D. *Phys. Rev. A: Gen. Phys.* **1988**, *38*, 3098.

(22) Perdew, J. P. *Phys. Rev. B: Condens. Matter Mater. Phys.* **1986**, *33*, 8822.

(23) Dolg, M.; Wedig, U.; Stoll, H.; Preuss, H. *J. Chem. Phys.* **1987**, *86*, 866. Wedig, U.; Dolg, M.; Stoll, H.; Preuss, H. In *Quantum Chemistry: The Challenge of Transition Metals and Coordination Chemistry*; Veillard, A., Ed.; D Reidel Publishing Co.: Dordrecht: The Netherlands, 1986; Vol. 176, pp 79–89.

(24) Szilagy, R. K.; Winslow, M. J. *Comput. Chem.* **2006**, *27*, 1385.

(25) (a) Laaksonen, L. *J. Mol. Graph.* **1992**, *10*, 33. (b) Bergman, D. L.; Laaksonen, L.; Laaksonen, A. *J. Mol. Graph. Model.* **1997**, *15*, 301.

(26) DuBois, J. L.; Mukherjee, P.; Stack, T. D. P.; Hedman, B.; Solomon, E. I.; Hodgson, K. O. *J. Am. Chem. Soc.*, **2000**, *122*, 5775.

of precipitate had formed and was removed by filtration through Celite after diluting the reaction solution with diethyl ether (100 mL). The filtrate was treated with a 1.0 M solution of anhydrous HCl in ether ( $2 \times 50$  mL) which immediately resulted in the precipitation of the product as an HCl salt. The solids were collected on a frit and washed with petroleum ether ( $3 \times 50$  mL). These solids were suspended in a 4:1 mixture of THF/ $\text{CH}_3\text{CN}$ , excess ( $>4$  equiv) NaOMe was added, and the mixture was stirred for 2 h. The solvent was removed in vacuo. The sticky solids were extracted with petroleum ether (50 mL) and filtered through Celite. The solvent was removed from the filtrate under reduced pressure. The resultant tacky translucent solid was stirred in  $\text{CH}_3\text{CN}$  for 1 h, affording a tractable white solid (5.35 g, 68%) which was pure by NMR spectroscopy.  $^1\text{H}$  NMR (300 MHz,  $\text{CD}_2\text{Cl}_2$ ):  $\delta$  7.66 (t, 1H), 7.46 (m, 2H), 7.16 (m, 4H), 1.34 (s, 18H), 1.00 (d, 6H), 0.94 (d, 6H).  $^{13}\text{C}\{^1\text{H}\}$  NMR (75.5 MHz,  $\text{CD}_2\text{Cl}_2$ ):  $\delta$  145.9, 143.5, 128.8, 127.4, 126.7, 116.6, 39.6, 34.9, 31.9, 27.1, 24.9, 24.6.  $^{31}\text{P}\{^1\text{H}\}$  NMR (121 MHz,  $\text{CD}_2\text{Cl}_2$ ):  $\delta$  -53.1. Anal. Calcd for  $\text{C}_{36}\text{H}_{61}\text{NP}_2$ : C, 75.88; H, 10.79; N, 2.46; Found: C, 75.35; H, 10.20; N, 2.81. UV-vis (THF,  $\text{nm}(\text{M}^{-1} \text{cm}^{-1})$ ): 303 (20 700), 344 sh.

**Synthesis of  $\{(\text{Bu}_2\text{-PNP})\text{Cu}\}_2$  (4).** Mesityl-Cu (128 mg, 0.702 mmol) and  $(\text{Bu}_2\text{-PNP})\text{H}$  (400 mg, 0.702 mmol) were dissolved in petroleum ether and stirred for 12 h at ambient temperature. The emissive yellow solution was filtered through a glass microfilter, and the solvent was removed in vacuo. The bright yellow solid was stirred in  $\text{CH}_3\text{CN}$  for 1 h in the dark and collected on a frit. Drying of the solids in vacuo afforded a finely divided analytically pure yellow solid (400 mg, 90%). Crystals suitable for XRD were obtained by slow evaporation of the solvent from a solution of **4** in THF.  $^1\text{H}$  NMR (300 MHz,  $\text{C}_6\text{D}_6$ ):  $\delta$  7.43 (m, 4H), 7.02 (m, 8H), 2.12 (n, 8H), 1.84–1.50 (m, 16H) 1.34 (s, 36H), 1.15 (d, 12), 0.89 (dd, 24), 0.76 (d, 12H).  $^{13}\text{C}\{^1\text{H}\}$  NMR (75.5 MHz,  $\text{C}_6\text{D}_6$ ):  $\delta$  168.1, 139.5, 128.5, 128.2, 127.1, 125.4, 40.0, 36.3, 34.6, 32.3, 26.7, 26.5, 25.9, 25.8.  $^{31}\text{P}\{^1\text{H}\}$  NMR (121 MHz,  $\text{C}_6\text{D}_6$ ):  $\delta$  -35.3. Anal. Calcd for  $\text{C}_{72}\text{H}_{120}\text{Cu}_2\text{N}_2\text{P}_4$ : C, 68.38; H, 9.56; N, 2.21. Found: C, 68.55; H, 9.38; N, 2.61. UV-vis (THF,  $\text{nm}(\text{M}^{-1} \text{cm}^{-1})$ ): 295 (20 500), 318 (21 100), 357 (33 300), 383 sh, 433 (4600), 459 (3800).

**Synthesis of  $\{(\text{Bu}_2\text{-PNP})\text{Cu}\}_2[\text{B}(\text{C}_6\text{H}_3(\text{CF}_3)_2)_4]$  (5).** Complex **4** (150 mg, 0.144 mmol) and  $[\text{Cp}_2\text{Fe}][\text{B}(\text{C}_6\text{H}_3(\text{CF}_3)_2)_4]$  (144 mg, 0.137 mmol) were combined in a 20 mL reaction vial and dissolved in  $\text{CH}_2\text{-Cl}_2$  (10 mL). The reaction immediately turned red-brown in color, and stirring was continued for 30 min at which time the solvent was removed in vacuo. The resultant solids were washed with petroleum ether ( $2 \times 10$  mL), extracted into diethyl ether (7 mL), filtered through a glass microfilter, and layered with petroleum ether. Analytically pure red crystals (203 mg, 78%) suitable for XRD were obtained after two successive recrystallizations from diethyl ether/petroleum ether at  $-35$  °C. Anal. Calcd for  $\text{C}_{88}\text{H}_{100}\text{BCu}_2\text{F}_24\text{N}_2\text{P}_4$ : C, 55.53; H, 5.30; N, 1.47. Found: C, 55.73; H, 5.21; N, 1.39. UV-vis ( $\text{CD}_2\text{Cl}_2$ ,  $\text{nm}(\text{M}^{-1} \text{cm}^{-1})$ ): 260 (sh), 309 (14 900), 359 (sh), 416 (2930), 529 (1090), 583 (sh), 661 (sh), 818 (1520), 981 (2053), 1684 (4500).

**Synthesis of  $\{(\text{Bu}_2\text{-PNP})\text{Cu}\}_2[\text{SbF}_6]$  (5).** Complex **4** (165 mg, 0.131 mmol) and  $\text{AgSbF}_6$  (44.8 mg, 0.131 mmol) were combined in a

20 mL reaction vial and dissolved in THF (10 mL). The reaction immediately turned red-brown in color, and stirring was continued for 12 h, after which time the solution was filtered through a glass microfilter to remove the  $\text{Ag}^0$  byproduct. The solvent was removed from the filtrate under reduced pressure, and the resultant red solids were extracted into  $\text{CH}_2\text{Cl}_2$  (4 mL), filtered, and layered with petroleum ether. After 2 days, analytically pure red crystals (159 mg, 81%) were obtained. Anal. Calcd for  $\text{C}_{72}\text{H}_{120}\text{Cu}_2\text{F}_6\text{N}_2\text{P}_4\text{Sb}$ : C, 57.63; H, 8.06; N, 1.87. Found: C, 57.64; H, 8.03; N, 2.17. Evans' method ( $\text{CD}_2\text{Cl}_2$ , 298 K): 1.63  $\mu_B$ . UV-vis ( $\text{CD}_2\text{Cl}_2$ ,  $\text{nm}(\text{M}^{-1} \text{cm}^{-1})$ ): 260 (sh), 312 (22 360), 377 (sh), 430 (3810), 510 (2280), 586 (sh), 639 (sh), 804 (1510), 941 (940), 1788 (5490).

**Synthesis of  $\{(\text{Bu}_2\text{-PNP})\text{Cu}\}_2[\text{SbF}_6]$  (6).** Complex **4** (100 mg, 0.079 mmol) and  $\text{NOSbF}_6$  (42 mg, 0.18 mmol) were combined in a 20 mL reaction vial and dissolved in  $\text{CH}_2\text{Cl}_2$  (10 mL). Upon dissolution, the solution immediately became red-brown in color then became blue after 10 min. After an additional 3 h of stirring, the solution was concentrated to 3 mL, filtered through a glass microfilter, and layered with petroleum ether (15 mL). Cooling the mixture to  $-35$  °C for 4 days caused a deep blue solid to precipitate. Two successive recrystallizations of **6** from petroleum ether/ $\text{CH}_2\text{Cl}_2$  at  $-35$  °C afforded an analytically pure, blue microcrystalline solid (65 mg, 47%) suitable for XRD studies. Modest yields result from multiple recrystallizations to ensure purity and are not reflective of a low conversion to product. Anal. Calcd for  $\text{C}_{72}\text{H}_{120}\text{Cu}_2\text{F}_{12}\text{N}_2\text{P}_4\text{Sb}_2$ : C, 49.81; H, 6.97; N, 1.61. Found: C, 49.41; H, 6.96; N, 1.76. Magnetic susceptibility ( $\text{CD}_2\text{Cl}_2$ , 298 K): 1.69  $\mu_B$ . UV-vis ( $\text{CD}_2\text{Cl}_2$ ,  $\text{nm}(\text{M}^{-1} \text{cm}^{-1})$ ): 294 (16 500), 321 (sh), 346 (21 700), 426 (sh), 510 (sh), 574 (sh), 620 (12 900), 1297 (300).

**Acknowledgment.** Financial support provided by the DOE (PECASE; J.C.P.); the ONR (N00014-06-1016; R.K.S.); and a NSF Graduate Research Fellowship (N.P.M.). Larry Henling and Dr. Mike Day provided crystallographic assistance. Portions of this research were carried out at the Stanford Synchrotron Radiation Laboratory, a national user facility operated by Stanford University on behalf of the U.S. Department of Energy, Office of Basic Energy Sciences. The SSRL Structural Molecular Biology Program is supported by the Department of Energy, Office of Biological and Environmental Research, and by the National Institutes of Health, National Center for Research Resources, Biomedical Technology Program.

**Supporting Information Available:** Synthesis and crystallography; DFT calculations; supplemental Cu K-edge spectra of two- and four-coordinate  $\text{Cu}^{\text{I}}$  complexes; complete ref 20. This material is available free of charge via the Internet at <http://pubs.acs.org>.

JA076537V